

Energy harvesting via co-locating horizontal- and vertical-axis wind turbines

M. Hansen¹, P. Enevoldsen² and M. Abkar¹

¹Department of Engineering, Aarhus University, Denmark

²Department of Business Development and Technology, Aarhus University, Denmark

E-mail: abkar@eng.au.dk

Abstract. Co-locating horizontal- and vertical-axis wind turbines has been recently proposed as a possible approach to enhance the land-area power density of wind farms. In this work, we aim to study the benefits associated with such a co-location using large-eddy simulation (LES) and analytical wake models. In this regard, small-scale vertical-axis wind turbines (VAWTs) in triangular clusters are deployed within a finite-size wind farm consisting of horizontal-axis wind turbines (HAWTs). Wake flow within the wind farm and the effect of VAWTs on the overall wind-farm efficiency are investigated and quantified. The results show that the optimal deployment of small-scale VAWTs has a negligible impact on the performance of HAWT arrays while increasing the total power production. For the particular cases considered here, the power output of the co-located wind farm increases up to 21% compared to the baseline case in which only the HAWTs are present. A budget analysis of the mean kinetic energy is carried out to shed light on the impact of VAWTs on energy transport into the wind-farm wake. Also, by comparing to the LES results, it is shown that the analytical framework proposed here is able to accurately predict the power production of wind farms including both HAWTs and VAWTs. Finally, as a real-world application, potential benefits of deploying small-scale VAWTs inside the Horns Rev 1 wind farm are explored for various wind directions using the validated wake model. The results show potential for about an 18% increase in the wind-farm power production, averaged over all wind directions, for a particular VAWT layout investigated in this study.

1. Introduction

Wind-turbine wakes require a relatively large distance to be fully recovered. Hence, when wind turbines are deployed in clusters, the performance of waked turbines significantly decreases compared to wind turbines in the free stream (see the review of Ref. [1]). One possible approach to mitigate the power defect due to the wake interaction is to install wind turbines as far as possible from one another [2], which is further enforced by the development of rotor sizes throughout the past decades [3]. However, this approach requires significant amounts of land which in practice is not always feasible for several reasons ranging from the costs of acquiring the land to increased likelihood of social opposition [4, 5].

Historically, wind farms were assumed to consist of identical horizontal-axis wind turbines (HAWTs). Recent studies have proposed a paradigm shift in which size and type of turbines is also a decision variable in the farm-design process [6–10]. Feng and Shen [8] investigated the benefits of wind farms consisting of HAWTs with multiple types using analytical wake models. They showed a lower energy cost for a wind farm with different sizes compared to a uniform-sized wind farm. Vassel-Behag and Archer [9] assessed the impact of hub-height optimization

on wind-farm energy extraction. They found that a wind farm with variable hub heights can produce >2% more energy annually compared to the wind farm with a uniform hub height. The benefits of vertically staggered wind farms by varying HAWT hub heights were also studied recently by Zhang et al. [10]. Using large-eddy simulation (LES), they showed that vertical staggering enhances the energy production of turbines in the entrance/developing region of the farm. However, this approach does not improve the power output in the fully developed regime.

A different approach is to fill the gap between large-scale HAWTs by deploying smaller vertical-axis wind turbines (VAWTs) [11]. VAWTs are a class of turbines with rotational axes perpendicular to the free stream, and have received a great deal of attention in recent years (see for instance Refs. [12–15], among others). Recently, Xie et al. [16] performed LES of an infinite wind farm (i.e., numerically subjected to periodic boundary conditions) consisting of co-located HAWTs and VAWTs. They showed that the small-scale VAWTs enhance the vertical momentum exchange within the farm leading to a significant increase (up to 32%) in the total wind-farm power. Despite the promising findings reported in that study, the aerodynamic interaction of co-located HAWTs and VAWTs in a finite-size wind farm is unknown and has not been studied so far. Note that for a small number of wind turbines or at the leading edge of a large wind farm, the energy is mainly extracted from the incoming wind due to the horizontal flux of kinetic energy [17]. Given the finite size of existing farms, investigating the impact of co-locating HAWTs and VAWTs on the overall performance of wind farms is valuable and is the central focus of this work.

The present work aims at exploring wake flow and generated power from a finite-size wind farm consisting of co-located HAWTs and VAWTs using LESs and analytical wake models. Section 2 provides a brief description of the LES and analytical frameworks for modeling wake flow through HAWTs and VAWTs. In Section 3, the impact of co-location on the wake flow and the total power production of the farm is examined, and the results are compared to the baseline case in which only HAWTs are present. Finally, the power enhancement by adding small-scale VAWTs to the Horns Rev 1 wind farm, as an existing wind farm, is investigated for various wind directions. In Section 4, a summary and concluding remarks are given.

2. Modelling

2.1. Large-eddy simulation framework

The previously-validated LES framework presented here (see for instance Refs. [18–21]) solves the filtered continuity and Navier-Stokes equations for incompressible turbulent flow,

$$\frac{\partial \tilde{u}_i}{\partial x_i} = 0, \quad \frac{\partial \tilde{u}_i}{\partial t} + \frac{\partial (\tilde{u}_i \tilde{u}_j)}{\partial x_j} = -\frac{1}{\rho_o} \frac{\partial \tilde{p}}{\partial x_i} - \frac{\partial \tau_{ij}}{\partial x_j} - \frac{f_i}{\rho_o}, \quad (1)$$

where \tilde{u}_i and \tilde{p} are the filtered velocity and pressure fields, respectively. x_i indicates the Cartesian coordinates. t is time. ρ_o is the fluid density. $\tau_{ij} = \widetilde{u_i u_j} - \tilde{u}_i \tilde{u}_j$ denotes the kinematic subfilter stress tensor. f_i is a body force and accounts for the effect of wind turbines on the flow. The code employs a pseudo-spectral discretization in horizontal directions, and a central finite difference method in the vertical direction. The second-order Adam-Bashforth scheme is applied for time advancement. The molecular viscous forces are neglected away from the wall, hence the flow is at nominally infinite Reynolds number. The subfilter turbulent motions are modeled via the scale-dependent Lagrangian dynamic approach [22]. The actuator-disk model with rotation [18] and the actuator swept-surface model [13] are respectively used to parameterize the forces induced by HAWTs and VAWTs. Through these approaches, the aerodynamic forces on the rotors are determined using the blade airfoil geometry, the relative wind velocity, and the lift-drag force characteristics of the blades. The inflow condition is generated through a precursor method and by simulating a turbulent flow over a rough surface. The computational domain size is 4800m × 1200m × 456m in the streamwise (x), lateral (y) and wall-normal (z)

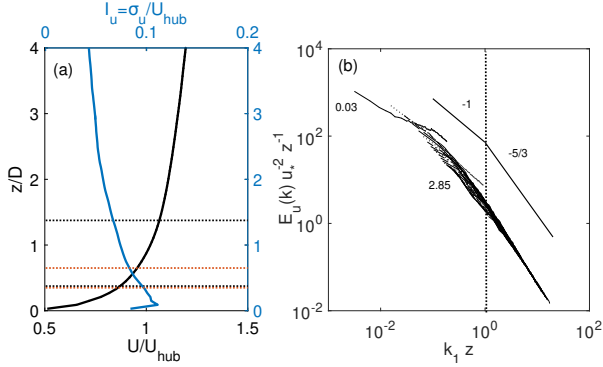


Figure 1: (a) Vertical profiles of the normalized mean streamwise velocity U/U_{hub} and the turbulence level $I_u = \sigma_u/U_{hub}$ for the incoming free stream. Horizontal black and red dot-lines show the HAWT and VAWT extents, respectively. (b) Normalized resolved streamwise velocity spectra. Here, u_* is the friction velocity, and the normalized height z/D increases from 0.03 to 2.85.

directions, respectively, and it is broken uniformly into $480 \times 240 \times 96$ grid points. An imposed uniform pressure gradient drives the boundary-layer flow in the streamwise direction. The effective ground roughness (z_o) is 0.05m, and the wall shear stress is specified following the equilibrium wall model. Further details of the solver can be found in Ref. [23].

The main characteristics of the incoming wind including the mean velocity, turbulence intensity and power spectra of the streamwise velocity component are shown in Fig. 1. The free-stream mean velocity at the HAWT hub-height U_{hub} is about 7.3m/s. The streamwise turbulence level $I_u = \sigma_u/U_{hub}$ at the same height is about 7.4%, where σ_u is the standard deviation of the streamwise velocity. Figure 1b illustrates the normalized spectra of the simulated streamwise velocity field obtained from the precursor simulation. As can be seen in this figure, the normalized power spectra depict the expected collapse for the small resolved scales ($k_1 z > 1$) and follow the theoretical scaling in the inertial subrange with a slope of $-5/3$. In the wake-flow simulation, a fringe zone is implemented to adopt the flow from the wake state downstream to that of a fully turbulent boundary-layer inflow condition [19].

The HAWTs used in the simulations are Vestas V80 turbines with the rotor diameter (D) of 80m and the hub height (z_h) of 70m. Details of the Vestas V80 wind turbine such as distributions of twist angle and chord length along the blades, and lift-drag coefficients as a function of angle of attack can be found in Ref. [18]. The VAWTs immersed in the flow are 200kW T1-turbines, which are the three- and straight-bladed VAWTs with the rotor diameter (D_v) of 26m, the blade span (H_v) of 24m, and the equator height (z_{hv}) of 40m. The blades of VAWTs consist of the standard NACA 0018 airfoil with the chord length of 0.75m, and the turbines operate at the nominal tip-speed ratio of 3.8 [20]. The thrust coefficients of the HAWTs and VAWTs are respectively around 0.8 and 0.64. A schematic of the HAWT and VAWT is shown in Fig. 2.

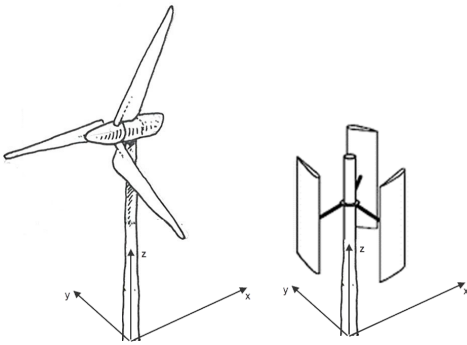


Figure 2: A schematic of a HAWT (left), and a three- and straight-bladed VAWT (right).

2.2. Analytical framework

The reduction of the mean wind velocity inside the wake is described by the normalized velocity deficit as $\Delta U/U_\infty = (U_\infty - U_w)/U_\infty$, where U_∞ is the turbine inflow velocity, and U_w is the wind velocity at a given position inside a wake. In this study, we use the recently-introduced Gaussian wake model for both HAWTs [24, 25] and VAWTs [20, 26]. The Gaussian wake model describes the wake velocity deficit as

$$\frac{\Delta U}{U_\infty} = C(x) \times \exp\left(-\frac{1}{2} \left[\left(\frac{y}{\sigma_y}\right)^2 + \left(\frac{z - z_h}{\sigma_z}\right)^2 \right]\right), \quad (2)$$

where C is the maximum velocity deficit, and σ_y and σ_z are respectively the spanwise and wall-normal standard deviations of velocity deficit distribution. The maximum velocity deficit in the wake is given by $C = 1 - \sqrt{1 - C_t/[2\pi(\sigma_y\sigma_z/A_p)]}$. Here, the turbine thrust coefficient is denoted by C_t . A_p is the turbine projected area, and is equal to $\pi D^2/4$ and $D_v H_v$ for HAWTs and VAWTs, respectively. As shown in the earlier studies [24, 26], for wind turbines in the turbulent free stream, a linear growth of the wake with downwind distance can be assumed, $\sigma_y = k^*x + \epsilon L_y$ and $\sigma_z = k^*x + \epsilon L_z$, where k^* denotes the wake expansion rate, and the characteristic turbine dimensions in the y and z directions are respectively labeled as L_y and L_z . In particular, $L_y = L_z = D$ for HAWTs, and $L_y = D_v$ and $L_z = H_v$ for VAWTs [26]. The wake expansion rate k^* is estimated based on the empirical formula suggested in Ref. [27] as $k^* = 0.35I_u$. ϵ in the equation above characterizes the wake standard deviation at the rotor, and it is defined as $\epsilon = 0.25\sqrt{\beta}$, where $\beta = 0.5(1 + \sqrt{1 - C_t})/\sqrt{1 - C_t}$ [24]. Note that, in the very far-wake region where $k^*x > \epsilon L_{y,z}$, the velocity deficit distribution by definition asymptotes to a circular shape from an elliptic shape as $\sigma_y/\sigma_z \rightarrow 1$. To account for multiple wake interactions within a wind farm, rotor wakes can be superposed in either linear or nonlinear manner [28, 29]. Based upon the linear superposition, the wake velocity within the farm can be estimated as $U_i = U_\infty - \sum_k (U_k - U_{ki})$ where U_i is the velocity at turbine i , U_k is the incoming velocity at turbine k , and U_{ki} is the wake velocity caused by turbine k at downstream turbine i . The velocity field emerged from multiple wake interactions can be alternatively modeled using the nonlinear superposition method as $U_i = U_\infty - \sqrt{\sum_k (U_k - U_{ki})^2}$. In the following section, the performance of the above-mentioned superposition methods is assessed using the LES data. The generated power by turbine i is determined as $P_i = 0.5\rho_0 C_p A_p U_i^3$, where C_p is the power coefficient of the turbine.

2.3. Wind-farm layout

Figure 3 illustrates the schematic of the wind-farm layout for the two cases considered in this study. Case (0) is the baseline case with no VAWT. The HAWTs are arranged in six columns and three rows in the streamwise and lateral directions, respectively. The distance among the HAWTs in the streamwise and lateral directions is $7D$ and $5D$, respectively. As mentioned before, deployment of wind turbines as far apart is required to mitigate the wake loss in wind farms. However, the available energy passing through the gap between large HAWTs is not accessible by them. In order to increase the land-area power density of wind farms, the gap between large HAWTs can be filled by the smaller VAWTs [4]. There are different ways to fill the gap between HAWTs using VAWTs, and several design parameters such as geometry, number, and exact location of VAWTs can be essentially optimized in order to maximize the benefits of wind-farm co-location. In this study, we consider one particular case to show the potential benefits of this approach in improving the power production of an existing wind farm. Case (1) represents a layout in which VAWTs are installed in triangular clusters in the free space among HAWTs. Here, the center of VAWT cluster is placed between each row and column of HAWTs in order to minimize the interaction between them. Each VAWT cluster consists of

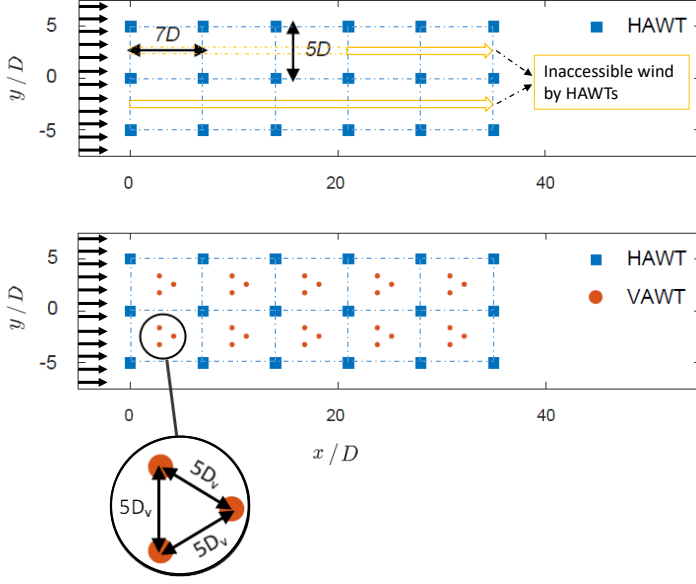


Figure 3: Wind-farm layout: Case (0): baseline (top) and Case (1): VAWT clusters between HAWTs (bottom).

three turbines with center-to-center distance among them of about $s_v D_v = 5D_v$. The selected configuration for the VAWT clusters is motivated by the recent study by Hezaveh et al. [30] who showed that the performance of VAWTs can be increased using synergetic clustering. In particular, by optimizing the VAWT numbers and the distance among them, they showed that such a configuration results in higher power production over a wide range of wind direction. As can be visually acknowledged in Fig. 3, the distance between VAWT clusters in the streamwise and lateral direction is $7D \simeq 21.5D_v$ and $5D \simeq 15.4D_v$, respectively, and the first column of VAWT clusters is placed $3.5D$ downstream of the first HAWT column.

3. Results

Here, we present the results obtained from the LES and the analytical wake model. In particular, we focus on analyzing the mean wake flow through the wind farm as well as the generated power by wind turbines for the two scenarios described in Section 2.3.

3.1. Case (0): HAWT farm

Figure 4 illustrates contour plots of the normalized instantaneous and time-averaged streamwise velocity at the HAWT hub height obtained from LES. As expected, the waked turbines encounter a reduced wind velocity and, consequently, produce less power compared to the turbines in the first column. Figure 5 represents the power efficiency as a function of turbine columns. Here, the power efficiency of each column is calculated as $\eta_c = P_c / P_{c,free}$, where P_c is the power output of all turbines in each column, and $P_{c,free}$ is the power output of all HAWTs in the first column operating in the free stream. The first column has all the turbines in the free stream and, hence, $\eta_c = 1$. Due to the wake effect, the efficiency drops by around 50% for turbines in the downstream columns. In this figure, the predictions obtained from the analytical wake model with linear and nonlinear superposition methods are also provided for comparison. As can be seen, the linear addition of the wake velocity defects leads to an underestimation of the power output for the downwind wind turbines. On the other hand, there is a good agreement between LES and the analytical model with nonlinear wake superposition. These results are consistent with previous studies that show the nonlinear superposition method can provide a more accurate prediction for the power production of wind turbines subjected to multiple wake interactions (see for instance the review of Refs. [31, 32], among others). In the analytical wake

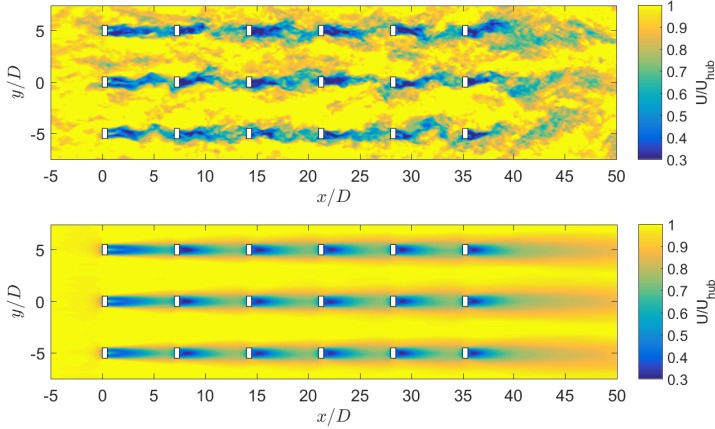


Figure 4: Instantaneous (top) and time-averaged (bottom) streamwise velocity field at HAWT hub height obtained from LES for Case (0).

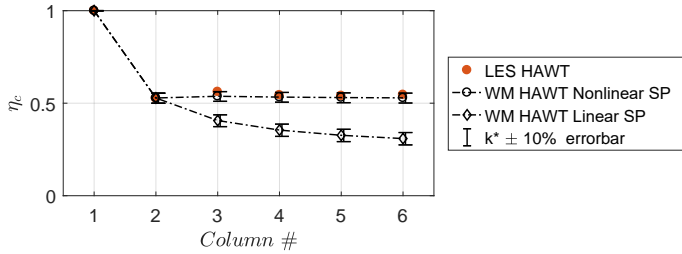


Figure 5: Power efficiency as a function of turbine columns for Case (0) obtained from LES and wake model (WM) with different superposition (SP) methods.

model, we also investigate the uncertainty in estimating the wake growth rate, k^* , as it is the only empirically-tuned parameter in the wake model. Here, we present the results with 10% uncertainty in the estimation of this parameter. It is found that 10% uncertainty in the wake growth rate leads to about 2.3% uncertainty in the power prediction of waked wind turbines. Since the analytical model with the nonlinear wake superposition provides a relatively accurate prediction for the power output in the baseline case, this method is used in the rest of the paper.

3.2. Case (1): Co-located VAWT clusters and HAWTs

In this case, HAWTs are kept in the same position as Case (0), and VAWT clusters are placed in the gap among them. Figure 6 show the contours of the normalized mean flow at HAWT and VAWT hub heights, respectively, obtained from LES. At the HAWT hub height, VAWT wakes appears far downstream of the farm, since the wake behind VAWTs needs to grow sufficiently in the vertical direction before being visible at the HAWT hub height. It can be also realized from these figures that the wakes of VAWT clusters are almost fully recovered before the next column since the relative distance between the two columns of VAWT clusters is relatively large (around $21.5D_v$).

The average turbine power efficiency for the turbines in each column is plotted in Fig. 7. The total power efficiency of the co-located wind farm is also plotted in this figure to illustrate the gain potential due to the presence of VAWTs. In order to better quantify the effect of VAWTs on the performance of HAWTs and on the total power output of the farm, we define the gain/loss factor as follows. The gain/loss factor in the power production of HAWTs due to the presence of VAWTs is defined as $\zeta_{HAWT,n} = \sum P_{HAWT,n} / \sum P_0 - 1$, where $\sum P_{HAWT,n}$ is the total power of HAWTs in Case (n) and $\sum P_0$ is the total power of HAWTs in the baseline case (i.e., Case 0). We also define the gain factor for VAWTs as $\zeta_{VAWT,n} = \sum P_{VAWT,n} / \sum P_0$, where $\sum P_{VAWT,n}$ is the total power of VAWTs in Case (n). Then, the net gain/loss factor is defined as $\zeta_{net,n} = \zeta_{HAWT,n} + \zeta_{VAWT,n}$. Note that, based on the definitions above, the gain/loss factor for Case (0) is zero. The gain/loss factor for the co-located wind farm is provided in Table

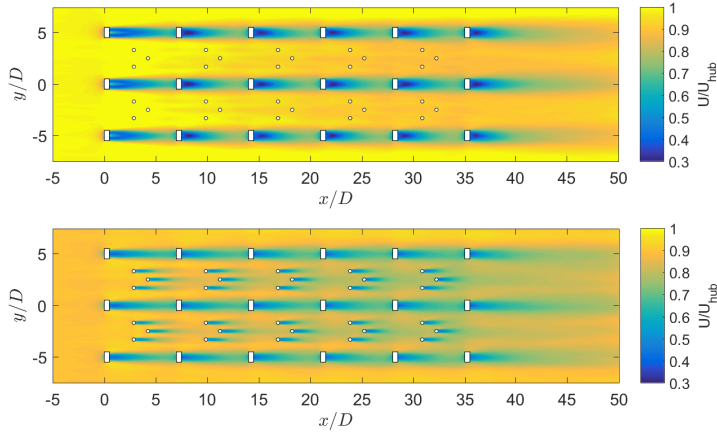


Figure 6: Time-averaged stream-wise velocity field at HAWT (top) and VAWT (bottom) hub heights obtained from LES for Case (1).

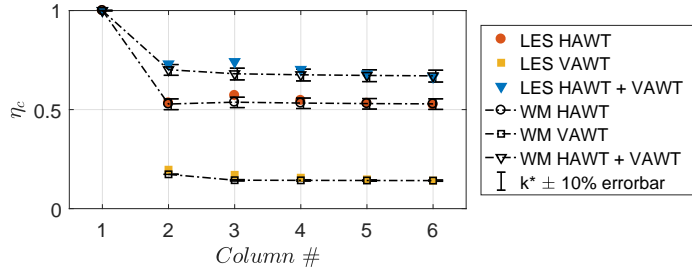


Figure 7: Power efficiency as a function of turbine columns for Case (1) obtained from LES and wake model (WM).

Table 1: Gain/loss factor for Case (1) obtained from LES.

I_u	ζ_{HAWT}	ζ_{VAWT}	ζ_{net}
7.4%	-0.7%	21.8%	21.1%

1. As can be noticed, the VAWTs have a relatively small impact on the performance of HAWTs by decreasing the HAWT farm efficiency by 0.7%. The slight reduction of the HAWT farm efficiency is related to the presence of VAWTs and their wake interactions with the HAWTs as shown in Fig. 6. However, these interactions are relatively small. Besides, due to the additional power generated by the VAWTs, the total power output is increased by 21.1% compared to the baseline case. Note that optimizing the design and placement of VAWTs can further reduce their negative impacts on HAWTs, and thus it can be addressed in future works. Also, similar to the previous results, a relatively good agreement between the LES data and the wake model is observed in predicting power efficiency for both the HAWTs and VAWTs.

3.3. Kinetic energy budgets of the mean flow

To better quantify the influence of VAWTs on the energy extraction from the turbulent incoming flow, a budget analysis of the mean kinetic energy for the wake flows through the wind farm is performed. As shown in previous studies [33–35], this analysis can shed light on the physics of energy exchanges between the incoming flow and turbine wakes. Under the steady-state condition, the kinetic energy budget of the mean flow can be written as

$$\underbrace{\frac{\partial (\bar{u}_j \bar{K})}{\partial x_j}}_{Adv.} + \underbrace{\frac{\partial \left[\bar{u}_j \bar{p} / \rho_o + \bar{u}_i \left(\bar{\tau}_{ij} + \overline{\tilde{u}'_i \tilde{u}'_j} \right) \right]}{\partial x_j}}_{T_t} = \underbrace{\left(\bar{\tau}_{ij} + \overline{\tilde{u}'_i \tilde{u}'_j} \right) \frac{\partial \bar{u}_i}{\partial x_j}}_{-P_s} - \underbrace{\frac{\bar{u}_i \bar{f}_i}{\rho_o}}_{W_t}, \quad (3)$$

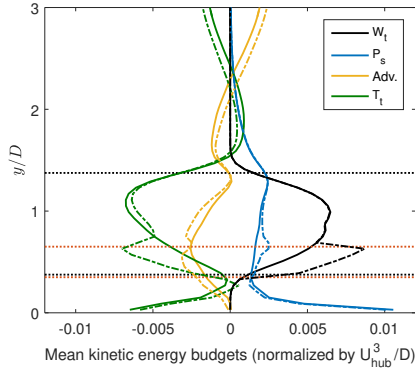


Figure 8: Mean kinetic energy budgets for Case (0) (solid line) and Case (1) (dash-dotted line).

where the overbar shows temporal averaging, $\tilde{u}'_i = \tilde{u}_i - \bar{u}_i$. $\bar{K} = 0.5\bar{u}_i\bar{u}_i$ is the kinetic energy of the mean flow. The *Adv.* term describes the advection of the mean kinetic energy by the mean flow, T_t represents the mean kinetic energy transport via pressure and turbulence. P_s is the turbulent kinetic energy production, and W_t is the work extracted by the turbines. In Fig. 8, the mean kinetic energy budget terms, averaged horizontally over the whole wind-farm domains, are shown. As can be seen, the turbulence production and the work done by the wind turbines increase inside the farm due to the presence of VAWTs. It can be also observed that, in order to balance the additional power output and turbulence production induced by the VAWTs, both transport and advection of the mean kinetic energy increase for Case (1) compared to the Case (0). It can be also seen that the higher values for advection and transport terms are mainly occur within the layer that the VAWTs are present. This result shows that the presence of the small-scale VAWTs enhances the total power extraction by increasing the advection and transport of mean kinetic energy from the boundary-layer flow.

3.4. Horns Rev 1 wind-farm power enhancement

As a real-world application, the benefits of co-locating HAWTs and VAWTs are investigated in the Horns Rev 1 wind farm under different wind directions. To do so, the analytical wake model, validated in the previous section, is employed. The Horns Rev 1 wind farm consists of 80 Vestas V80 HAWTs in 8 rows by 10 columns grid with a minimum distance among two turbines (s) of 7 HAWT rotor diameter. Columns are turned 7° from the North-South axis. A schematic of the wind farm is shown in Fig. 9. The type of turbines is the same as the ones used in previous cases. The incoming wind velocity at the HAWT hub height is 8m/s. To assess the effect of atmospheric turbulence on the results, three different values for the ambient turbulence intensity are considered as $I_u = 5\%$, 7.7% and 15% . VAWTs are deployed based on the same layout concept as Case (1), i.e., VAWT triangular clusters in the gap between the HAWTs. In order to provide a more complete picture of the effect of VAWTs on the HAWT array, wind-farm efficiency in all wind directions is investigated. Due to the symmetry of the wind-farm layout, it is sufficient to investigate wind directions ranging over 180° . Here, we define the efficiency of the entire wind farm as $\eta = \sum P / \sum P_{free}$, where $\sum P$ is the sum of power output from all wind turbines, and $\sum P_{free}$ is the total power output from HAWTs calculated as if they were placed in the free stream.

Figure 9 shows the wind-farm power efficiency, η , for wind directions ranging from $173^\circ - 353^\circ$ obtained from wake model with 10% uncertainty in the wake growth rate. The wind-farm power output obtained from LES in the absence of VAWTs [36] is also included for comparison. As can be seen, a relatively good agreement between the LES and the wake model is observed, especially for wind directions with lower power efficiency under full-wake conditions. In other wind directions, under partial-wake regimes, the wake model overestimates the power efficiency

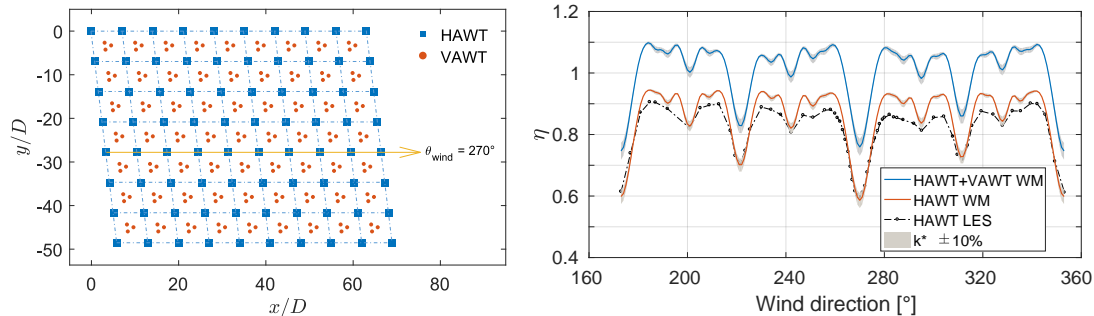


Figure 9: Left: Layout of the Horns Rev 1 wind farm. The HAWTs and VAWTs are respectively shown with blue squares and red circles. Right: Power efficiency distribution of the Horns Rev 1 wind farm with VAWT clusters. The ambient turbulence level is 7.7%. LES data were digitally extracted from Ref. [36].

Table 2: Gain/loss factor for the Horns Rev 1 case averaged over all wind directions.

I_u	ζ_{HAWT}	ζ_{VAWT}	ζ_{net}
5%	-1.4%	17.9%	16.5%
7.7%	-1.0%	18.3%	17.3%
15%	-0.6%	18.8%	18.2%

of the farm. It should be noted that, although there are some discrepancies between the LES and wake model, in this study, we aim to investigate the relative improvement of wind-farm power production due to the presence of VAWTs. Adding the VAWTs to the wind farm shows a similar trend in power efficiency as the one discussed earlier. The effect of small-scale VAWTs on the HAWTs is relatively small, while they produce additional wind power. It can be also seen that, for all wind directions, the efficiency of the co-located wind farm is higher than the baseline case. To better quantify the impact of VAWTs on the HAWT farm, the gain/loss factor under different ambient turbulence levels is provided in Table 2. For the particular wind-farm layout considered here, the power production of the farm (averaged over all wind directions) increases by 16.5%, 17.3% and 18.2% for the ambient turbulence intensity of 5%, 7.7% and 15%, respectively. It is interesting to observe that the ambient turbulence level has a relatively small effect on power enhancement due to the turbine co-location. In addition, it is found that 10% uncertainty in the wake growth rate yields about 1% uncertainty in estimating the total power production averaged over all wind directions which is much smaller than the gained power due to the presence of VAWTs. This result reveals the potential to enhance the wind-power density of wind farms by co-locating VAWTs and HAWTs.

4. Conclusion

The benefits associated with co-locating HAWTs and VAWTs in a finite-size wind farm are investigated in this study. In this regard, LES together with the analytical wake model is employed. Small-scale VAWTs in triangular clusters are deployed within a finite-size wind farm consisting of conventional HAWTs. For the particular cases studied here, the potential power gain in the wind farm with both HAWTs and VAWTs is up to 21% compared to a baseline case in which only HAWTs are present. The budget analysis of the mean kinetic energy are performed to elucidate the effect of VAWTs on the energy transport into the wind farm wake. This analysis reveals that the presence of VAWTs enhances the advection and the transport of mean kinetic energy leading to a higher energy extraction from the wind turbines. It is also shown that the impact of small-scale VAWTs on the performance of HAWTs is relatively small if the VAWTs are

deployed properly among HAWTs. Furthermore, the performance of the analytical framework is evaluated using the LES data, and it is found that the presented analytical framework is able to accurately predict the power output from wind farms consisting of both HAWTs and VAWTs. Finally, the validated analytical wake model is used to investigate the potential power enhancement in the Horns Rev 1 wind farm by adding small-scale VAWTs over a wide range of wind directions. It is shown that by adding the small-scale VAWTs to the wind farm, the power production can increase by up to 18% (averaged over all wind directions). We conclude that co-locating conventional HAWTs and small-scale VAWTs is a promising approach to increase the land-area power density in existing wind farms. Future research is required to optimize the design and placement of clustered VAWTs within HAWT arrays to maximize the power production of co-located wind farms.

Acknowledgments The work is financially supported by Aarhus University.

References

- [1] Stevens R J and Meneveau C 2017 *Ann. Rev. Fluid Mech.* **49** 311–339
- [2] Meyers J and Meneveau C 2012 *Wind Energy* **15** 305–317
- [3] Enevoldsen P and Xydis G 2019 *Energy Sustain. Dev.* **50** 18–26
- [4] Sivaram V, Dabiri J O and Hart D M 2018 *Joule* **2** 1639–1642
- [5] Enevoldsen P, Valentine S V and Sovacool B K 2018 *Energy Policy* **120** 1–7
- [6] Vested M H, Hamilton N, Sørensen J N and Cal R 2014 *J. Phys.: Conf. Ser.* **524** 012169
- [7] Chamorro L P, Tobin N, Arndt R and Sotiropoulos F 2014 *Wind Energy* **17** 1483–1494
- [8] Feng J and Shen W Z 2017 *Appl. Energy* **205** 1283–1297
- [9] Vassel-Be-Hagh A and Archer C L 2017 *Appl. Energy* **195** 905–921
- [10] Zhang M, Arendshorst M G and Stevens R J 2018 *Wind Energy* **22** 189–204
- [11] Dabiri J O, Greer J R, Koseff J R, Moin P and Peng J 2015 *AIP Conf. Proc.* **1652** 51–57
- [12] Dabiri J O 2011 *J. Renew. Sustain. Energy* **3** 043104
- [13] Shamsoddin S and Porté-Agel F 2014 *Energies* **7** 890–912
- [14] Bianchini A, Balduzzi F, Bachant P, Ferrara G and Ferrari L 2017 *Energy Convers. Manag.* **136** 318–328
- [15] Rezaeiha A, Montazeri H and Blocken B 2018 *Energy* **165** 1129–1148
- [16] Xie S, Archer C L, Ghaisas N and Meneveau C 2016 *Wind Energy* **20** 45–62
- [17] Abkar M and Porté-Agel F 2014 *Renew. Energy* **70** 142–152
- [18] Wu Y T and Porté-Agel F 2015 *Renew. Energy* **75** 945–955
- [19] Abkar M and Porté-Agel F 2015 *Phys. Fluids* **27** 035104
- [20] Abkar M and Dabiri J O 2017 *J. Turbul.* **18** 373–389
- [21] Abkar M 2018 *Atmosphere* **9** 257
- [22] Bou-Zeid E, Meneveau C and Parlange M 2005 *Phys. Fluids* **17** 025105
- [23] Yang X and Abkar M 2018 *J. Fluid Mech.* **842** 354–380
- [24] Bastankhah M and Porté-Agel F 2014 *Renew. Energy* **70** 116–123
- [25] Abkar M, Sørensen J and Porté-Agel F 2018 *Energies* **11** 1838
- [26] Abkar M 2019 *Energies* **12** 10
- [27] Carbaño Fuertes F, Markfort C D and Porté-Agel F 2018 *Remote Sens.* **10** 668
- [28] Lissaman P 1979 *J. Energy* **3** 323–328
- [29] Voutsinas S, Rados K and Zervos A 1990 *J. Wind Eng. Ind. Aerodyn.* **14** 204–219
- [30] Hezaveh S H, Bou-Zeid E, Dabiri J, Kinzel M, Cortina G and Martinelli L 2018 *Boundary-Layer Meteorol.* **169** 275–296
- [31] Göçmen T, Van der Laan P, Réthoré P E, Diaz A P, Larsen G C and Ott S 2016 *Renew. Sustain. Energy Reviews* **60** 752–769
- [32] Archer C L, Vassel-Be-Hagh A, Yan C, Wu S, Pan Y, Brodie J F and Maguire A E 2018 *Appl. Energy* **226** 1187–1207
- [33] Abkar M and Porté-Agel F 2016 *Phys. Rev. Fluids* **1**(6) 063701
- [34] Cortina G, Calaf M and Cal R B 2016 *Phys. Rev. Fluids* **1** 074402
- [35] Bastankhah M and Abkar M 2019 *Phys. Fluids* **31** 085106
- [36] Niayifar A and Porté-Agel F 2016 *Energies* **9** 741